Downwash Detection and Avoidance with Small Quadrotor Helicopters

Derrick W. Yeo,* Nitin Sydney,† and Derek A. Paley ‡

University of Maryland, College Park, Maryland, MD 20742, U.S.A

Donald Sofge §

Naval Research Laboratory, Washington, DC 20375 , U.S.A

I. Introduction

By using four independent rotors to provide lift and control moments, the quadrotor helicopter provides researchers with a small, mechanically simple and effective vertical-flight platform. Typically, the lift and resultant torque due to each rotor can be approximated with simple aerodynamic models. Although these models have proven to be adequate in low advance-ratio flight conditions [1], they cannot account for the flow conditions associated with high-speed flight or the presence of large disturbances such as wind gusts or downwash from nearby rotorcraft. Real-time measurements of the flow-field around a flying vehicle provide a description of the flight conditions that would otherwise be impossible with only inertial-based instruments.

This paper introduces a pressure-probe flow measurement system developed for a small quadrotor. The design, fabrication and calibration of the instrumentation package are presented along with data from autonomous flight trials using motion-capture-based positioning data. As a demonstration of the capabilities afforded by onboard flow sensing, a strategy for avoiding the downwash of a neighboring rotorcraft is proposed and demonstrated.

Assimilating vertical flow-field measurements with a Bayesian estimation algorithm detects and localizes the source of vertical flow disturbances for use in a flight-path planner developed for proximity flight. The path planner minimizes a cost function that drives the vehicle to a desired waypoint while avoiding the

*Research Associate, Department of Aerospace Engineering, dyeo@umd.edu , AIAA Member.
†Ph.D Candidate,Department of Aerospace Engineering, nsydney@umd.edu , AIAA Student Member.
‡Willis H. Young Jr. Associate Professor of Aerospace Engineering Education, Department of Aerospace Engineering, and the Institute for Systems Research dpaley@umd.edu, AIAA Senior Member.
§Computer Scientist, Naval Research Laboratory, donald.sofge@nrl.navy.mil , AIAA Member.

vertical downwash. Test results from indoor experiments with two quadrotors operating at different altitudes showcase the capability of the flight planner to generate trajectories that successfully avoid the downwash of a second rotorcraft.

The contributions of the research described in this paper are (1) implementation of an onboard flow sensing instrumentation system that uses an array of distributed pressure sensors to produce measurements of the surrounding flow-field; and (2) a flight-path planner that localizes the source of downwash in order to generate a safe trajectory to a desired goal location. The measurements from the instrumentation system are used in a recursive Bayesian estimator to estimate the position of another quadrotor, which in turn is used in the path planner for guidance and control.

The rest of the paper is as follows. Section II provides background of onboard flow sensing for small-scale flyers. Section III describes the design and testing of the airspeed instrumentation system. Section IV presents a recursive Bayesian estimator that estimates the position of a hovering quadrotor using downwash measurements. Section VI contains results from experimenting with a flight-path planner for proximity flight. Section VII summarizes the paper and ongoing work.

II. Background

The use of flow sensing has been employed with great success on naturally evolved flyers [2]. Using distributed measurements of relative wind, sufficiently large creatures such as birds align themselves with their intended direction of travel and account for the effects of wind gusts. By detecting fine details of the ambient flow-field, small creatures like insects improve their flight performance by finely tuning their flap stroke to suit flight conditions[2]. Gewecke and Woike [3] showed that directing airflow over avian feathers could cause steering impulses and, as shown in more recent work by Brown and Fedde[4], birds have the necessary feather-sensor mechanisms in the wing to predict stall and measure airspeed.

In contrast to natural flyers, the current paradigm of small UAS instrumentation is to integrate inertial measurements supplemented by (scalar) airspeed. A five-hole probe providing air-data measurements that include airspeed, angle of attack, and sideslip has been successful in applications involving conventional fixed-wing flight within the traditional flight envelope [5, 6, 7]. These platforms provide a baseline capability for more advanced tests in areas such as cooperative control [8] and ocean-borne operations [9] for both fixed-wing and rotary-wing vehicles [10, 11].

Seeking improved platform performance, researchers have looked to expand the notion of onboard flow sensing and apply it to various levels of vehicle control. For example, flow information can be used to fine-tune aerodynamic parameters for performance. Patel and Corke [12, 13] considered the time-domain response from a high-bandwidth pressure sensor to predict incipient flow separation at the wing leading edge

and trigger a plasma flow actuator to alleviate flow separation.

Flow sensing can also improve flight control. Xu et al. [14] implemented arrays of micro-machined shear-stress sensors on the leading edge of a low aspect-ratio delta wing. The sensor system was developed to support control strategies that effected aerodynamic flight control through boundary-layer manipulation [15]. The AVOCET project [16] aims to continuously tailor the pressure distribution and resulting forces and moments across the wing using advanced micro-tuft sensors and hybrid fluidic flow actuators. Under attached flow conditions, NASA has supported wind tunnel-based implementation and testing of a distributed actuation and sensing array for use on a blended-wing-body UAV, using a series of pressure measurements to study the effectiveness of a morphing-wing control strategy [17, 18]. More recently, Mohamed et al [19] have demonstrated turbulence mitigation through the use of flow measurements taken in fron of the main wings.

At the path-planning level, aerodynamic sensing provides information that can drive vehicle configuration or guidance decisions based on flight conditions. For example, Cox et al. [20] used pressure based estimates of the lift curve above an airfoil as feedback for an automated cruise flap. Yeo et al. [21] used real-time stall detection through pressure sensing to change controller modes on a small, fixed-wing UAV during transition between forward flight and propeller-borne hover.

The work presented in this paper seeks to expand the notion of onboard aerodynamic sensing for small rotorcraft UAVs. Additional flow information across the rotors promises to improve quadrotor attitude stabilization in wind [22], while also detecting environmental disturbances for improved trajectory planning. This paper focuses on aerodynamic sensing as an enabler for improved multiple vehicle operations, which often require close-proximity flight.

Recently, there have been several approaches proposed for dealing with proximity flight [22, 23, 24, 25]. For example [22], a nonlinear controller that uses estimates of the wind speed to compensate for a rotor downwash impinging on the vehicle. However, the controller assumes knowledge of the structure of the downwash. In another example [25], a controller is designed to compensate for minor (1-2 m/s) changes in airspeed due to quadrotors operating at the same altitude. In both examples, the external wind (or an estimate of the wind) impinging on the rotorcraft is assumed to be available.

External wind information is provided in this paper by a novel probe-based flow measurement package. Unlike traditional measurement techniques employed on small rotors such as hot-wire anemometry [12] and optical velocimetry methods [13, 17, 20], the pressure-probe-based approach used here is inherently portable, rugged and well-suited for implementation onboard a small flight vehicle. The instrumentation system presented in this work is capable of providing flow speed measurements below 5 m/s in real-time, enabling the implementation of flow-based guidance and control. To show the utility of the instrumentation system,

we design a flight-path planner to avoid downwash of another quadrotor while simultaneously directing the vehicle toward a goal location.

III. Quadrotor Instrumentation System

The flow instrumentation system shown in Fig. 1 uses custom-built pressure probes that provide flow information through differential-pressure measurements. A single top-mounted airspeed probe takes measurements along the longitudinal and lateral directions of the vehicle and four vertical-airspeed probes are mounted uniformly around the vehicle outside the downwash the rotors. A two-port, fore- and aft-facing configuration allows for low flow speeds to be measured with improved signal-to-noise ratio as compared to a standard pitot-static probe configuration.

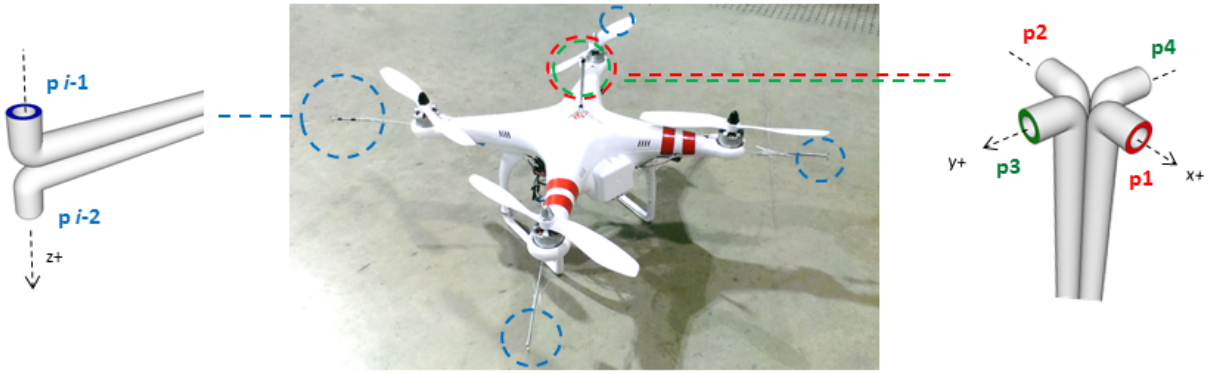

Figure 1. Quadrotor flow instrumentation: probe locations and geometry

The instrumentation packages are portable and easily mounted on a variety of small quadrotor vehicles. The probes are constructed out of aluminum tubing that is bent to form two to four pressure ports at each tip. The probe design is based on a multi-hole probe for propeller-wash measurements [10]. The design, geometry and port configuration of the various probes is shown in Fig. 1. Each pressure port pair provides a single differential pressure measurement that is used to compute the airspeed component along the ports by

$$u = L_u \sqrt{\frac{2L_b(P_1 - P_2)}{\rho}} \tag{1}$$

$$v = L_v \sqrt{\frac{2L_b(P_4 - P_3)}{\rho}} \tag{2}$$

$$w_i = L_{w_i} \sqrt{\frac{2L_b(P_{i,1} - P_{i,2})}{\rho}}, \tag{3}$$

where the scaling factors L_u, L_v and L_w are determined for each specific by calibration in a wind tunnel. These values varied between 0.96 and 1.05. The factor L_b accounts for the probe design and was experimentally determined to be 0.89. The subscript i denotes the four vertical velocity probes at each corner of the vehicle. The probes are calibrated between a 0-5m/s range for the low flight speeds anticipated in this work. The calibration is applied onboard and a moving-average filter is implemented. (The air data system is built around a Freescale Semiconductor MK20DX256VLH7 ARM Cortex M4 microprocessor running 13bit ADC at 1kHz. Honeywell HSCDRRN001NDAA3 differential pressure sensors are used to measure probe pressures and processed flow speed measurements are transmitted over a serial port interface.)

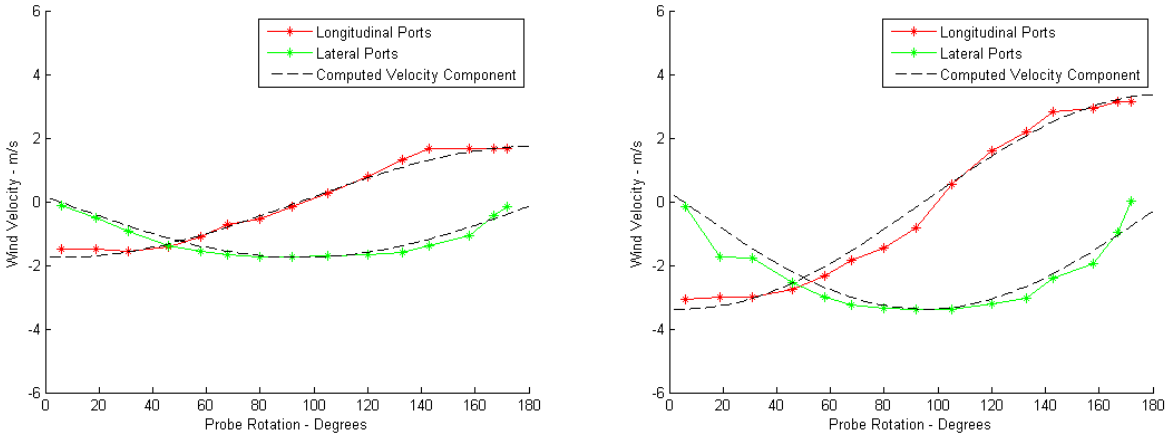

(a) 1.8 m/s Freestream

(b) 3.3 m/s Freestream

Figure 2. Wind tunnel tests: measured longitudinal and lateral airspeed components

The directional sensitivity of the port configuration was first evaluated through wind tunnel testing. The probe is mounted on a rotating stage that yaws the probe in a constant free stream. Measurements from both sets of ports were compared against idealized wind-vector values at each probe angle. Fig. 2 shows that the probe is able to estimate flow direction reasonably at airspeeds between with typical error under 0.5m/s.

The ability of the instrumentation package to provide wind-vector information in flight was also tested using remotely piloted maneuvers in an indoor motion-capture facility. A Blade 350QX was flown diagonally across the capture space to generate airspeed along the body-fixed lateral and longitudinal axes. Wind-vector measurements taken by the translational probe were streamed to a ground station and compared against ground-speed data from the motion-capture system, assuming still air.

Fig. 3 suggests that the pressure-port configuration is capable of providing reliable directional velocity

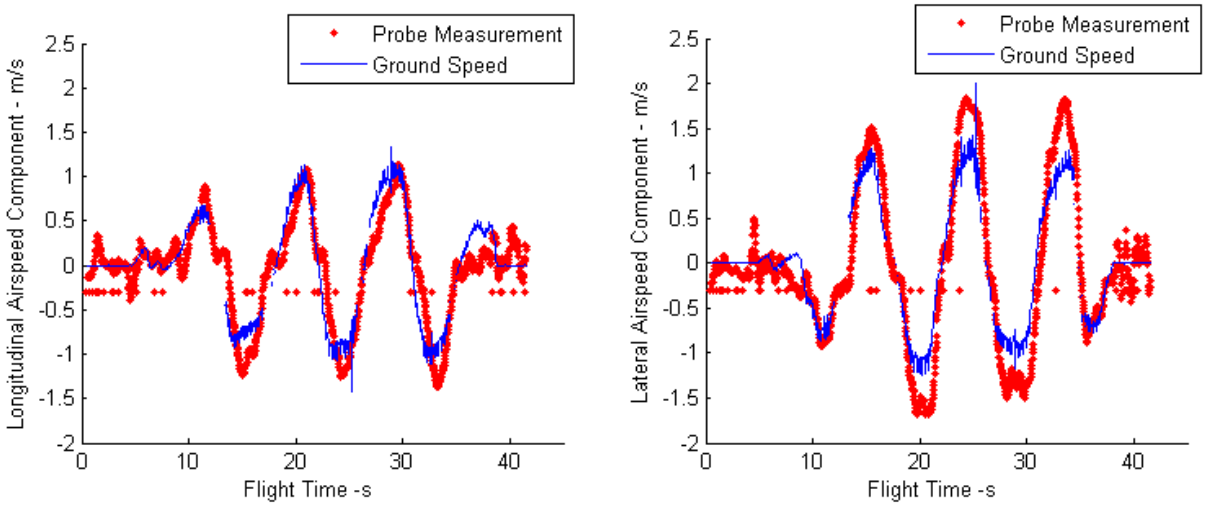

(a) Longitudinal component

(b) Lateral component

Figure 3. Remotely piloted flight tests: measured longitudinal and lateral airspeed components

measurements. Using a combination of one lateral airspeed probe and four vertical downwash probes, the instrumentation scheme is capable of providing relative wind-vector information over the body of the vehicle. This paper focuses on using the vertical wind-vector measurements to sense vertical flow disturbances.

IV. Localizing the Source of Rotorcraft Downwash

Vertical flow disturbances affect small-vehicle flight by creating transient disruptions to aerodynamic force generation. For multiple rotorcraft operating in close proximity, impinging downwash from a vehicle operating at a higher altitude causes sudden and possibly catastrophic loss of thrust from the affected rotor. Knowledge of the flow environment provides a flight controller with the data to accommodate and avoid such disturbances. This section summarizes the development of a Bayesian estimation scheme and accompanying vertical flowfield model that uses real-time flow measurements around a quadrotor to localize and avoid the downwash from another quadrotor.

Recursive Bayesian estimation provides a probabilistic framework for inferring an unknown quantity given a set of measurements [22]. An estimator is used here to continuously update the most likely location of an external source of downwash based on a set of vertical flow measurements. The location of the external source is denoted by $\beta = (x_s, y_s)$, where (x_s, y_s) are the inertial coordinates of a nearby rotorcraft operating at a higher altitude and creating a region of accelerated flow. We assume the instrumented quadrotor knows its own inertial position, but this is unnecessary as the estimates can also be used to compute relative positions. Let $\boldsymbol{z}(t_k)$ be a vector of noisy windspeed measurements taken using the flow measurement system at time t_k. The probability of β being the center of a vertical flow disturbance given the set of measurements up to t_k is

$$p(\beta|\boldsymbol{z}(t_1),..,\boldsymbol{z}(t_k)) = Ap(\boldsymbol{z}(t_k)|\beta)p(\beta|\boldsymbol{z}(t_1),..,\boldsymbol{z}(t_{k-1})), \tag{4}$$

where $p(\beta|\boldsymbol{z}(t_1),..,\boldsymbol{z}(t_k))$ is the posterior probability density and A is a normalization constant that gives the posterior unit integral. The likelihood function $p(\boldsymbol{z}(t_k)|\beta)$ represents the conditional probability of receiving measurements $\boldsymbol{z}(t_{k-1})$ from a nearby vehicle located at β. The mode $\hat{\beta}$ of (4) is the maximum likelihood estimate of the source of downwash.

Suppose there are N spatially distributed probes across the vehicle; the ith probe has the likelihood function $p(\boldsymbol{z}^i(t_k)|\beta)$, where $\boldsymbol{z}^i(t_k)$ is the measurement from the ith probe. The posterior based on all probe measurements is

$$p(\beta|\bar{\boldsymbol{z}}(t_k)) = p(\beta|\boldsymbol{z}(t_1),..,\boldsymbol{z}(t_{k-1}))\prod_{i=1}^{N} p(\boldsymbol{z}^i(t_k)|\beta), \tag{5}$$

where $\bar{\boldsymbol{z}}(t_k)$ comprises the measurements from all probes up to and including time t_k.

A key component in implementing a Bayesian estimator is a suitable likelihood function that uses knowledge of the expected flow-field to extract information pertaining to the environment from spatially distributed flow measurements. The likelihood function translates a vertical-velocity measurement to information pertaining to the location of a nearby vehicle through knowledge of the downwash it generates. Obtaining a simple flow model that adequately captures the key characteristics of a range of downwash flow is challenging as a rotor-driven flow-field is inherently complex, time-varying and characterized by a number of unknown parameters. A model for estimation should not require numerical simulation or significant prior knowledge about the flow. This requirement means existing flow models[26, 27] for small propellers are unsuitable for this work, motivating a first-order analysis of the governing flow equations.

Consider a two-dimensional flow-field with a rotor generating thrust along the z-axis. Velocity components w and v lie along the z and y coordinates respectively [28]. The momentum equation in the z direction is

$$\frac{\partial w}{\partial t} + w\frac{\partial w}{\partial z} + v\frac{\partial w}{\partial y} = g_z - \frac{1}{\rho}\frac{\partial p}{\partial z} + \frac{\mu}{\rho}\left(\frac{\partial^2 w}{\partial z^2} + \frac{\partial^2 w}{\partial y^2}\right) \tag{6}$$

where ρ is air density, μ is the dynamic viscosity of the air, and g_z represents body forces due to effects such as bouyancy. The following set of assumptions are applied as follows: (i) the mean flow-field is unchanging, so $\partial w/\partial t$ is zero; although rotorwash is highly turbulent, a rotorcraft in a steady flight condition will generate a steady mean flow-field velocity. (ii) Cross-stream flow is small compared to the downstream velocity; we only consider flow that is vertically oriented. For simplicity, only the thrust-aligned velocity component is considered and $\partial w/\partial y$ is neglected. (iii) At each z location, the stream-wise variation in w is small compared to the cross stream changes; hence, $\partial^2 w/\partial z^2$ is zero. (iv) Lastly, bouyancy and external pressure gradients

are not present, so g_z and $\partial p/\partial z$ are neglected.

Eq. (6) is further simplified by linearizing about a constant peak velocity W_0 based on the assumption that center-line flow velocities obey a $1/z$ decay as in a turbulent jet[28]. The result is

$$W_0 \frac{\partial w}{\partial z} = \frac{\mu}{\rho}\left(\frac{\partial^2 w}{\partial y^2}\right). \tag{7}$$

Solving (7) in cylindrical coordinates yields a Gaussian velocity profile reminiscent of the velocity variation observed in established turbulent jet profiles [29]. The expected vertical velocity measured at a lateral distance $r(\beta) = \sqrt{(x - x_s)^2 + (y - y_s)^2}$ and a downstream distance z from the center of an idealized rotorcraft is

$$w(\beta) = \frac{C}{z} W_0 \exp\left(-\frac{W_0 r(\beta)^2 \rho}{4 z \mu}\right). \tag{8}$$

The measurement $\boldsymbol{z}^i(t_k)$ of the ith sensor at time t_k is assimilated into the Gaussian likelihood function

$$p(\boldsymbol{z}^i(t_k)|\beta) = \exp((\boldsymbol{z}^i(t_k) - w)/\sigma^2), \tag{9}$$

where σ^2 is the variance of the measurement noise which is chosen based on measured velocity fluctuations.

Localization of a simulated downwash source was performed to validate the Bayesian estimation approach. The localization scheme is first evaluated with a single flow sensor approaching an idealized downwash source. The reduced-order model is used to generate both the estimated flow-field and the sequence of sensor measurements. Uncertainty is introduced through mismatches in model parameters and through process noise that represents velocity fluctuations present in actual measurements. Results from four time steps are shown in Fig. 4 The contour maps depict the posterior distribution of the location of the disturbance. Red indicates high probability, whereas blue indicates low probability. Red asterisks denote the measurement location. Fig. 4(d) also shows the path taken by the probe as it approaches the disturbance.

At t=0, the estimation scheme reports a probability of a downwash source within some radial distance of the sensor depending on the flow model and subject to the the measured turbulence level. Since the model only encodes radial distances, this single measurement cannot provide direction information and spatially distributed measurements are needed. For experimental validation with a static flow-field, successive measurements from a single moving sensor can be used. As measurements from different locations are assimilated, arcs of high probability are computed, resulting in a final estimate that is close to the center of the idealized downwash. Being able to assimilate multiple measurements from spatially distributed flow sensors offers advantages discussed in Section V.

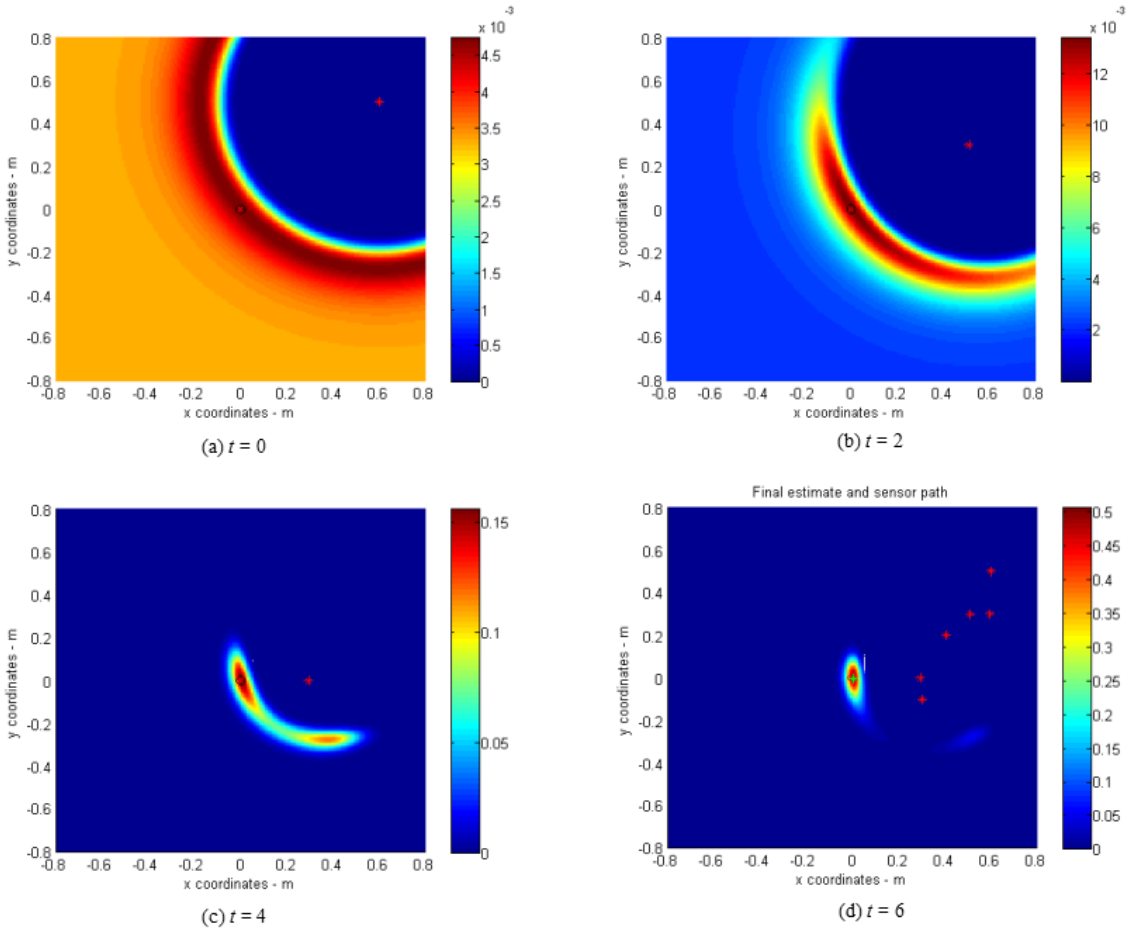

Figure 4. Simulated localization results with numerically generated flow measurements

V. Model Validation

The ability of the estimation strategy to localize the source of small rotorcraft downwash was evaluated through ground-based experiments. The downwash generated by an isolated propeller and a quadrotor helicopter was characterized and the estimation scheme tested within each flow-field. This section describes the automated test system and presents velocity measurement from the flow survey along with downwash localization results.

A Detrum 13inch propeller and a DJI Phantom quadrotor helicopter were suspended within a motion-capture facility. Custom electronics were installed on each test article to govern rotor RPM. A 2-axis Cartesian robot was built to position an air velocity probe within the flow using position feedback from the motion-capture system. A sliding carriage is driven over a guide rail with a servo-motor and drive wheel, providing translation in the inertial x-direction. The guide rail is itself propelled in the y-direction through a servo-motor powered winch and pulley system. Experiments are coordinated by a desktop computer that communicates with the motion capture system, drive actuators, and flow instrumentation. In addition to

providing repeatable sensor positioning within a volume of interest, this system allows a sensor payload to be guided through prescribed trajectories in a plane. A picture of the test setup and a breakdown of key components are shown in Fig. 5. Unlike conventional survey experiments [30], these tests are designed to capture representative data sets to validate the localization concept. The carriage uses a probe that shares the same design as the onboard instrumentation to take vertical flow velocity measurements within the downwash regions.

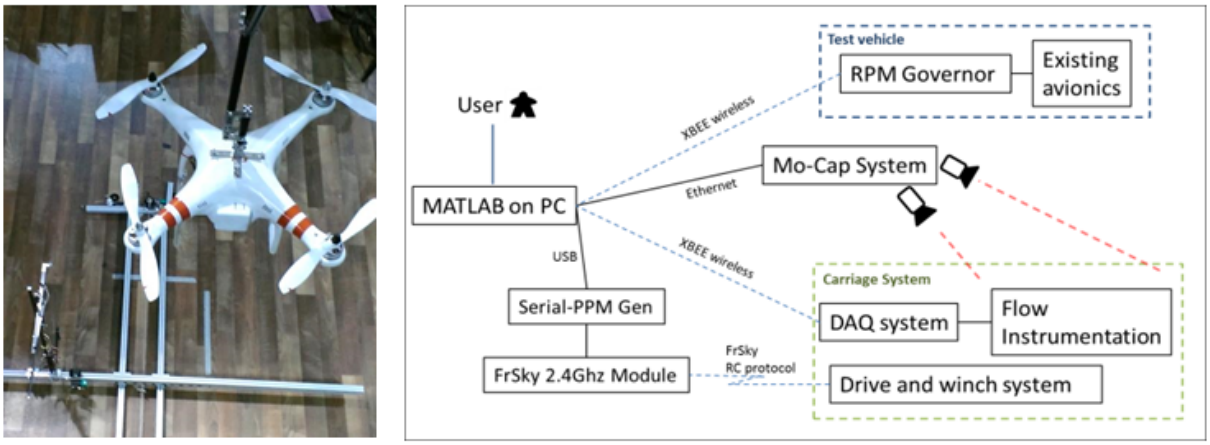

Figure 5. Automated flow survey apparatus and system overview

V.A. Downwash Survey Results

As a reference case, a two bladed 13x6 propeller was tested first. An isolated propeller generates an axisymmetric flow-field that is most similar to the downwash model and would provide insight as to the effects of flow turbulence on the estimation strategy. The propeller was rotated at 3500 RPM, corresponding to a tip Reynolds number of approximately 70,000. The test article, velocity surface and velocity contours at four propeller diameters downstream are shown in Fig. 6.

By using two pairs of counter-rotating propellers, the quadrotor helicopter configuration allows for a mechanically simple rotorcraft design with few moving parts. The vehicle used for these tests is a DJI Phantom, a small quadrotor that uses 8-inch diameter propellers. The velocity distributions at seven rotor diameters below the vehicle are shown in Fig. 7

V.B. Localization Results

The estimation scheme was tested within the flow generated by the isolated propeller and a quadrotor helicopter. The experimental data from the downwash surveys was used to evaluate the estimation strategy when subject to realistic flow-fields. In both cases, the probability density at the final time step is plotted

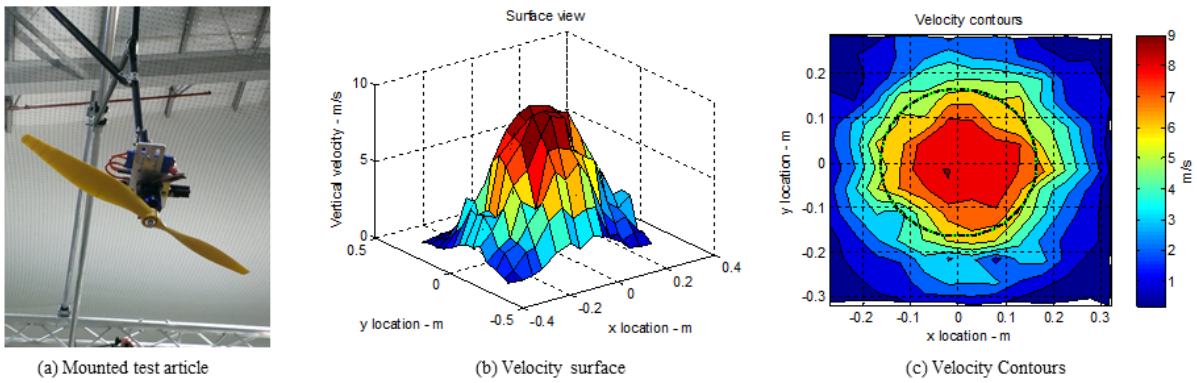

(a) Mounted test article (b) Velocity surface (c) Velocity Contours

Figure 6. Isolated propeller test overview

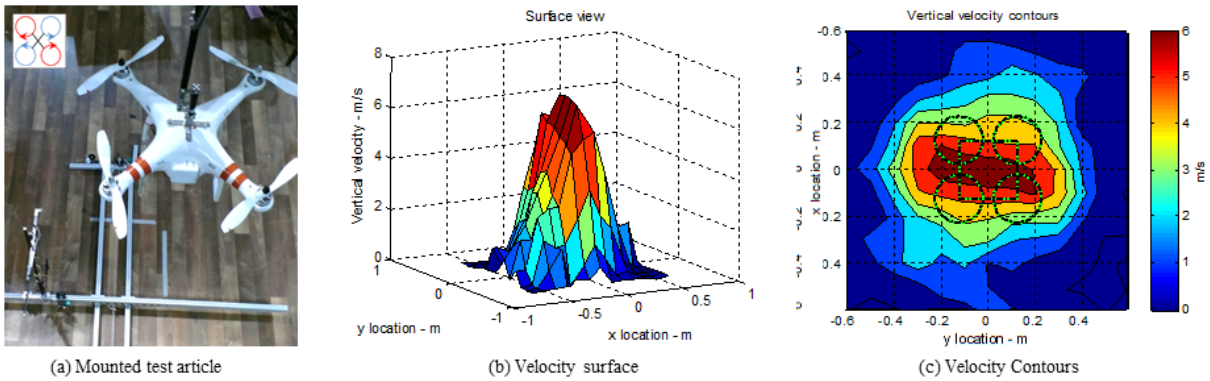

(a) Mounted test article (b) Velocity surface (c) Velocity Contours

Figure 7. Quadrotor helicopter test overview

with the location of the mode β marked by a green asterisk. The sequence of single sensor measurements is marked with red asterisks, and the footprint of the vehicle is outlined in green. Figure axes are aligned with the body frame of the test article, showing a view of the vehicle from the top with the nose of the vehicle facing the right side.

The estimation framework was first tested within the flow generated by a single propeller. Although the isolated propeller is axisymmetric, the sensor path was recreated to approach the propeller from the front and aft as a first-order verification of the system. These results are shown in Figs. 8(a) and 8(b), respectively. Note that variations in measured velocity and varying levels of turbulence between the measurement sets result in a slightly different final location estimates. Nonetheless, on both paths, the central location of the propeller is localized to within 15% of propeller diameter.

The elliptical velocity profiles beneath the quadrotor offers an additional level of complication in the estimation scheme since the flow-field is not axisymmetric. The velocity gradient recorded by a set of measurements depends on the orientation of the quadrotor and is not accounted for in the model. Two sensor

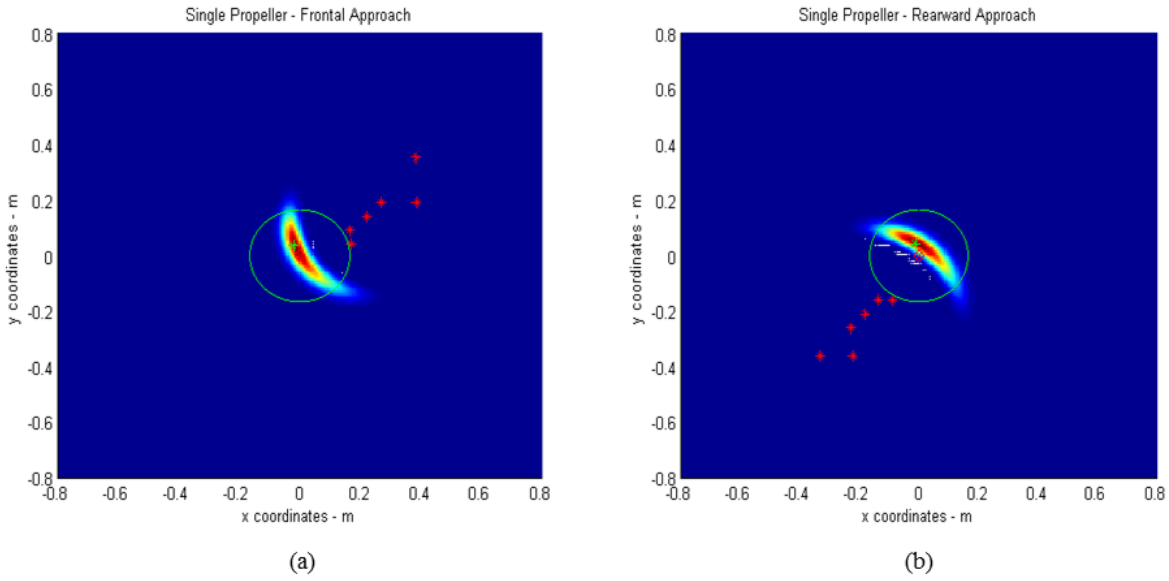

Figure 8. Isolated propeller estimation results

paths are chosen that approach the vehicle between both planes of symmetry. Estimates were generated within 30% of vehicle length and the localization results are shown in Fig. 9. These results were obtained using a set of generalized estimation parameters $\frac{W_0}{z} = 4.5$ and $C = 1.5$ that were experimentally developed using a range of small rotary wing vehicles[31].

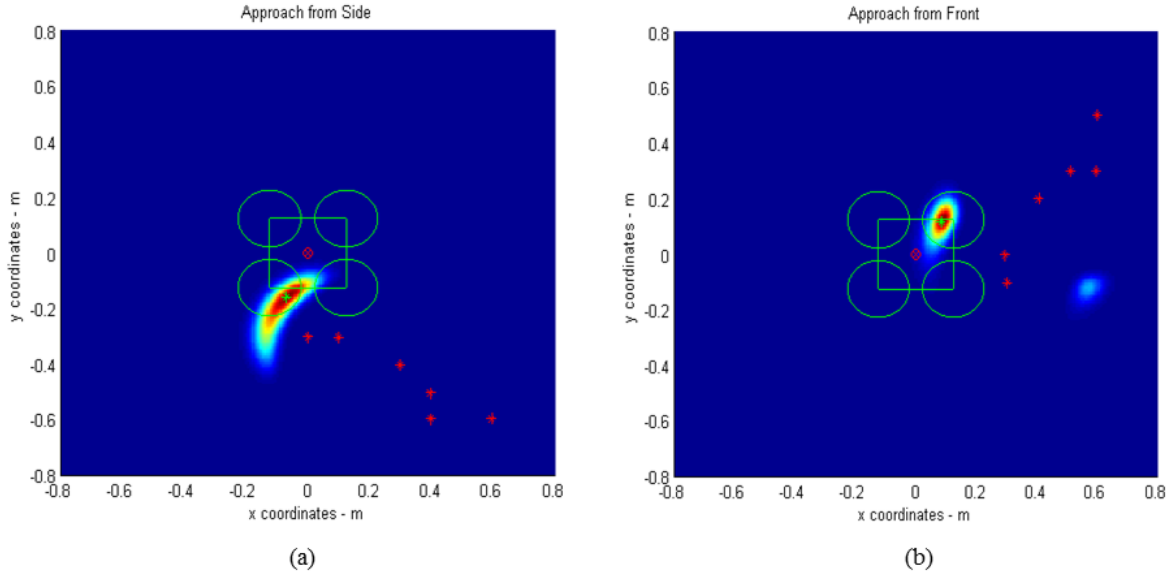

Figure 9. Quadrotor estimation results

Multiple, spatially distributed measurements at each time step enhances the accuracy of flow-field information. When mounted on a quadrotor helicopter, the instrumentation system includes four vertical flow probes around the vehicle. In these ground tests, two spatially distributed measurements are emulated by

combining the data from two single sensor runs. Multiple sensor runs from the side and front of a quadrotor are shown in Figs.10(a) and 10(b), respectively. In these plots, the locations of the second measurement are marked with a light blue asterisk.

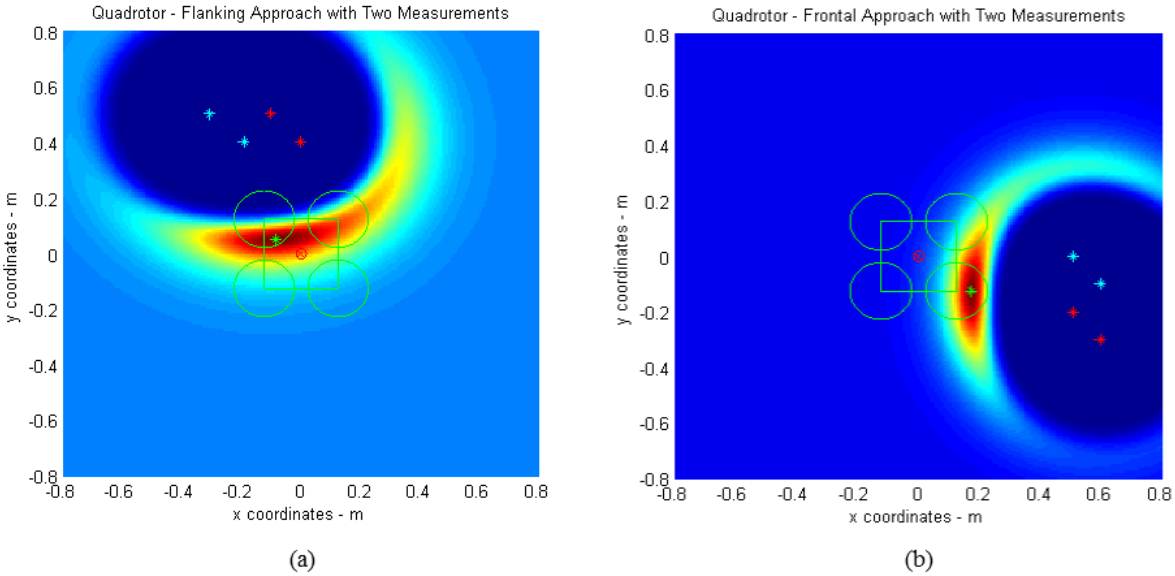

Figure 10. Estimation results with multiple sensors

In all ground test cases, the estimation scheme generated useful position estimates for different rotorcraft UAVs. The disturbance source was localized within the vehicle footprint without requiring measurements directly beneath it. The spatial resolution provided by assimilating data from two sensors improved the ability of the localization scheme to generate useful estimates from a longer range.

VI. Proximity-Flight Experimental Results

This section showcases the utility of a flow sensing and control system for proximity flight. The scenario involves two quadrotor's operating at different altitudes. The downwash of one quadrotor causes extreme, undesired changes in attitude and altitude of another quadrotor flying below[22]. The flight-path planner and flow measurement system were implemented on the lower quadrotor. The planner generates an estimate of the position of the higher quadrotor to determine the direction the lower quadrotor must travel to reach a desired waypoint while avoiding the downwash. The flow measurement system and path planner were validated in simulation and experiment.

As the quadrotors treated as stable platforms for the sake of path planning, consider an idealized vehicle

with the dynamics

$$\dot{x} = u_x \tag{10}$$

$$\dot{y} = u_y, \tag{11}$$

where x and y are the coordinates of the vehicle and u_x and u_y are control inputs. A 2D planner is sufficient for guidance in this scenario as we aim to de-conflict a vertical column of airspace, but the framework can be extended to 3D. The goal is to design u_x and u_y to drive the vehicle to a waypoint and avoid the vertical jet produced by the higher quadrotor. The cost function $J(x, y, t_k)$ incorporates the desired goal and the presence of a vertical flow-field, i.e.,

$$J(x, y, t_k) = p(\beta|\bar{\boldsymbol{z}}(t_k)) + k_J\sqrt{(x - x_d)^2 + (y - y_d)^2}, \tag{12}$$

where (x_d, y_d) is the location of the goal and k_J is a weighting variable. Intuitively, the cost is high when the vehicle is far away from the waypoint and/or near the downwash of the higher quadrotor. The goal is to find a path C through the domain such that the integral of J along the path is locally minimized. Formally, the problem is stated as

$$\begin{aligned} \underset{u_x,u_y}{\text{minimize}} \quad & \int_C J(x, y, t_k)ds \\ \text{subject to} \quad & \dot{x} = u_x \\ & \dot{y} = u_y, \end{aligned} \tag{13}$$

where ds is an increment along the path.

To decrease the computational complexity, a receding-horizon version of (13) looks only one time step ahead. In this case the cost function reduces to

$$J_{RH} = J(x, y, t_k) + J(x + \Delta x, y + \Delta y, t_k) \tag{14}$$

Since the first term on the right-hand side is fixed by the current vehicle location, the cost function is minimized by moving in the direction of greatest decrease. Thus, in the zero limit of Δx and Δy, (14) is minimized using the control

$$u_x = -K\frac{\partial J}{\partial x} \tag{15}$$

$$u_y = -K\frac{\partial J}{\partial y}, \tag{16}$$

where K is a control gain. This choice of control moves the vehicle in the direction of greatest decrease in cost.

The algorithm was first tested in simulation[32]. The first quadrotor was commanded to hover at an altitude of 2.5 m, and the instrumented quadrotor was given a waypoint at (2.0, 0.0) m. Fig. 11 shows the results of the simulation. Each subfigure shows a snapshot at a different time step, starting from the initial time until the vehicle reaches the goal. The colormap at the bottom shows the posterior distribution for the position of the hovering quad, with red and blue denoting high and low probability, respectively. The black dot indicates the position of the hovering quadrotor, the green dot is the position of the instrumented quadrotor, and the red X shows the destination of the instrumented vehicle. The trajectory of the quadrotor is shown as a white line on top of the posterior distribution. The estimate of the position of the hovering quadrotor is shown as a magenta dot. The results show that the instrumented quadrotor traveling towards the waypoint, then diverting once it detects the higher quadrotor using (simulated) flow measurement data. Note that the estimate does not achieve zero steady-state error due to virtual noise in the sensor measurements.

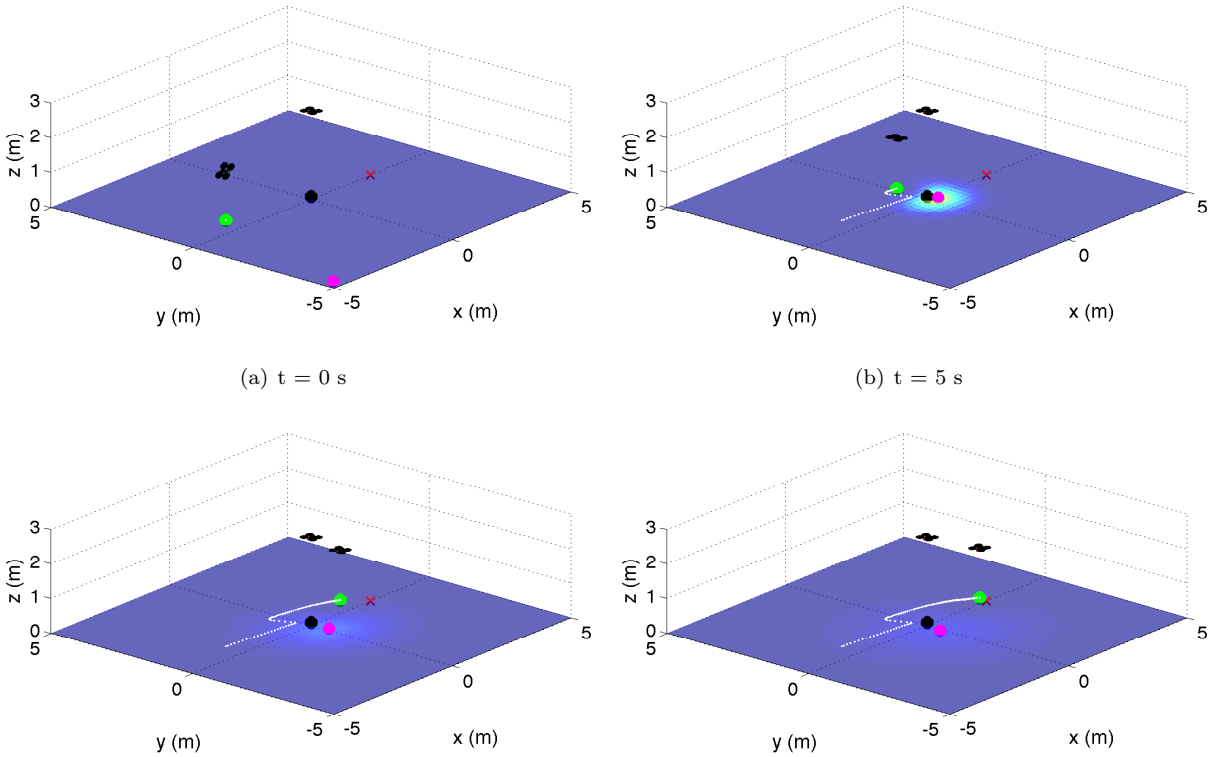

(a) t = 0 s

(b) t = 5 s

(c) t = 10 s

(d) t = 15 s

Figure 11. Trajectory of an instrumented quadrotor in proximity flight. The colormap indicates the posterior distribution of the probability of the hovering quadrotor location.

To validate the flow instrumentation system and proximity flight path planner, actual experiments were performed at the Naval Research Laboratory in the Laboratory for Autonomous Systems Research (LASR). The experiments were performed in a motion-capture testbed in the Prototyping Highbay at LASR, which

is 150 by 75 ft and equipped with 115 Vicon motion-capture cameras. Flight tests were conducted using two Ascending Technologies Pelican quadrotors. The Pelican has two onboard computers, one for flight stabilization and a Linux computer for sensor integration and control calculations. The Linux computer runs the Robot Operating System (ROS), which is a message-passing architecture for autonomous robots.

In the experiment, the high-altitude quadrotor was commanded to hover above the origin at an altitude of 2.5 m. The instrumented quadrotor was commanded to go to the waypoint (2.5, 0.0) m while an altitude of 1.5 m from five separate initial conditions. Fig. 12 shows the results of the flight test for all of the runs. Fig. 12(a) shows the trajectory of the two quadrotors. The black X indicates the position of the hovering quadrotor and the green X shows the desired waypoint. The dashed black circle shows the approximate area where the downwash of the hovering quadrotor is significant. The dashed red trajectory shows the path of the lower vehicle with control disabled to show the nominal trajectory the vehicle would take to the goal. (Note that for safety reasons the nominal trajectory was implemented without the presence of the hovering quadrotor.) The other trajectories show the quadrotor with the sensing and control system enabled. Fig. 12(b) shows the measurements (colored dots) taken by the flow measurement system for the red colored run as well as the estimation error (solid lines) of the hovering quadrotor's position for all five runs that included the hovering vehicle (the estimates are color coded to match the trajectories in Fig. 12(a)). Fig. 12(c) shows the x and y position estimates of the hovering quadrotor for the red run.

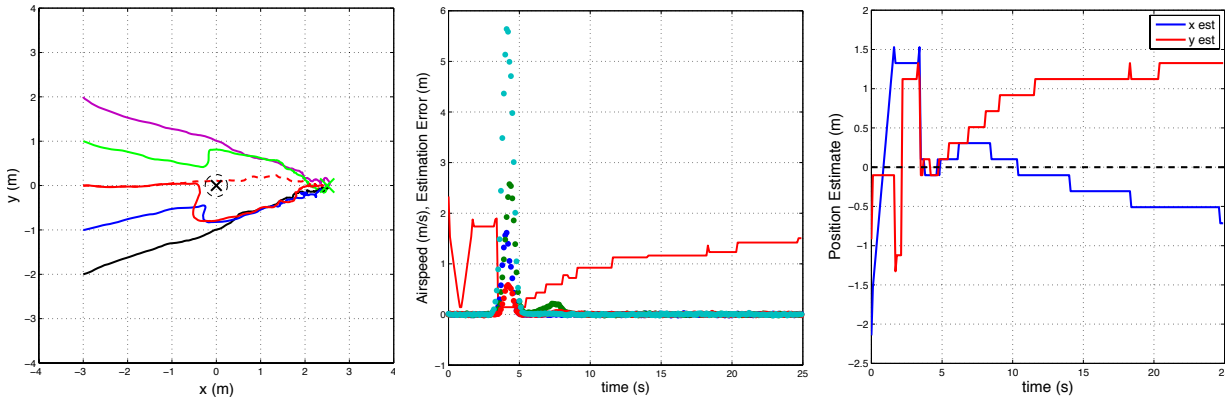

(a) (b) (c)

Figure 12. (a) Trajectory of the quadrotor from five separate initial conditions with the hovering vehicle located at the origin and one initial condition without the hovering vehicle. (b) measurements from the airspeed probes and hovering quadrotor estimation error for the red trial. (c) position estimate of the hovering quadrotor for the red run (middle trajectory)

The experiments illustrates the value of the flow measurement system and the flight-path planner. A vehicle without the combined system travels in a straight trajectory towards the waypoint, as indicated by the dashed red line in Fig. 12(a). This trajectory would place the vehicle directly under the downwash of the higher quadrotor. The vehicle with the flow measurement and flight-path planner detects the downwash of the higher quadrotor at approximately $t = 3.0$ seconds for the red, blue, and green trajectories, as seen

in Fig. 12(b). As soon as the sensor measures a positive airspeed, the error in the estimate of the position of the higher quadrotor begins to drop. Note that the error in the estimate is likely due to a combination of sensor noise and uncertainty in the choice of parameters in the likelihood function. Once the estimate of the higher quadrotors position converges, the instrumented vehicle maneuvers to avoid the downwash, as shown by the red, blue, and green trajectories in Fig. 12(a). The position estimates for the red run seen in Fig. 12(c) show how the estimate converges to near the correct value when the instrumented vehicle passes close to the hovering quadrotor. The estimate drifts away once the downwash is no longer detected, due to process noise that is added to the recursive Bayesian filter to account for possible motion of the downwash source. The magenta and black trajectories do not travel close enough to the hovering quadrotor to detect the downwash, which is apparent in Fig. 12(a) as the vehicle does not maneuver to avoid the downwash and the estimate never converges. This approach can be extended to a moving top aircraft by adding a motion prediction step in the estimation scheme.

VII. Conclusion

An onboard flow-sensing concept for quadrotor platforms is introduced along with an instrumentation package based on a set of custom wind-velocity probes. Data from ground-based tests and autonomous flight trials show that the system is capable of providing accurate wind-vector measurements in flight. A flight-path planner is designed to use these measurements to generate an estimate of the source of a downwash generated by a second rotorcraft; safe trajectories avoid hazardous downwash conditions. The flow measurement system and flight-path planner were tested in simulation and in a motion-capture testbed. Experiments showed that the vehicle was able to successfully avoid the downwash of another quadrotor and still reach a desired goal point. Ongoing work aims to develop an autopilot that incorporates flow-speed measurements into an attitude stabilization controller.

Acknowledgments

This work was performed at the University of Maryland and the Naval Research Laboratory and was funded by the US Department of Defense, Office of Naval Research under grant number N0001413WX21045, Mobile Autonomous Teams for Navy Information Surveillance and Search (MANTISS); U. S. Army under Grant No. W911W6112072; and the Air Force Office of Scientific Research under Grant No. FA95501310162, Dynamic Data Driven Applications Systems (DDDAS). The views, positions and conclusions expressed herein reflect only the authors opinions and expressly do not reflect those of the US Department of Defense, Office of Naval Research, or the Naval Research Laboratory.

References

[1] M. Belkheri, A. Rabhi, A. Hajjaji, and C. Pergard. Different linearization control techniques for a quadrotor system. In *2nd Int. Conf. on Communications, Computing and Control Applications,*, pages 1–6, December 2010.

[2] D. Alexander and S. Vogel. *Nature's Flyers: Birds, Insects, and the Biomechanics of Flight.* Johns Hopkins University Press, October 2004.

[3] M. Gewecke and Martin Woike. Breast feathers as an air-current sense organ for the control of flight behaviour in a songbird (carduelis spinus). In *Zeitschrift fr Tierpsychologie* ,, volume 47, pages 293–298, 1978.

[4] R. Brown and M. Fedde. Airflow sensors in the avian wing. In *Journal of Experimental Biology* ,, volume 179, pages 13–30, 1993.

[5] S. Herwitz, K. Allmendinger, R. Slye, S. Dunagan, B. Lobitz, L. Johnson, and J. Brass. Nighttime UAV vineyard mission: Challenges of see-and-avoid in the NAS. In *Proc. AIAA 3rd Unmanned Unlimited Conference, Workshop and Exhibit*, pages 1–6, September 2004.

[6] R. Beard, D. Kingston, M. Quigley, D. Snyder, R. Christiansen, W. Johnson, T. McLain, and M. Goodrich. Autonomous vehicle technologies for small fixed wing UAVs. In *AIAA Journal of Aerospace Computing, Information, and Communication*, volume 2, page 92, January 2005.

[7] R. Hirokawa, D. Kubo, S. Suzuki, J. Meguro, and T. Suzuki. Small UAV for immediate hazard map generation. In *AIAA Infotech@Aerospace Conf*, May 2007.

[8] F. Hsiao, Y. Ding, C. Chuang, C. Lin, and Y. Huang. The design of a small UAV system as a testbed of formation flight. In *AIAA Infotech@Aerospace Conf*, March 2011.

[9] R. Eubank, E. Atkins, and D. Macy. Autonomous guidance and control of the flying fish ocean surveillance platform. In *AIAA Infotech@Aerospace Conf*, April 2009.

[10] N. Rasmussen, B. Morse, and C. Taylor. Fixed-wing, mini-UAV system for aerial search operations. In *AIAA Guidance Navigation and Control Conference and Exhibit*, August 2007.

[11] P. Xie, A. Flores-Abad, G. Martinez, and O. Ma. Development of a small UAV with autopilot capability. In *Proc. AIAA Atmospheric Flight Mechanics Conference*, August 2011.

[12] M. Patel, Z. Sowle, T. Corke, and C. He. Autonomous sensing and control of wing stall using a smart plasma slat. In *Proc. 44th AIAA Aerospace Sciences Meeting*, January 2006.

[13] P.Bowles and T. Corke. Stall detection on a leading-edge plasma actuated pitching airfoil utiliizing onboard measurement. In *Proc. 47th Aerospace Sciences Meeting*, January 2009.

[14] Y. Xu, F. Jiang, S. Newbern, A. Huand, C. Ho, and Y. Tai. Flexible shear-stress sensor skin and its application to unmanned aerial vehicles. In *Sensors and Actuators A: Physical*, volume 105, pages 321–329, 2003.

[15] C. Gorsjean, G. Lee, W. Hong, Y. Tai, and C. Ho. Micro balloon actuators for aerodynamic control. In *Micro Electro Mechanical Systems, The Eleventh Annual International Workshop on*, pages 166–171. IEEE, January 1998.

[16] Air Force Office of Scientific Research (AFOSR). Multidisciplinary university research initiative grant fa9550-05-1- 0411 http://www.avocet.gatech.edu [retrieved 22 aug. 2013].

[17] W. Barnwell. Flight Control Using Distributed Actuation and Sensing. Master's thesis, North Carolina State University, USA, 2003.

[18] S. Lion. Control authorities of a distributed actuation and sensing array on a blended-wing-body uninhabited aerial vehicle. Master's thesis, North Carolina State University, USA, 2007.

[19] A. Mohamed, M. Abdulrahim, S. Watkins, and R. Clothier. Development and flight testing of a turbulence mitigation system for micro air vehicles. In *Journal of Field Robotics*, August 2015.

[20] C. Hall. C. Cox, A. Gopalarathnam. Flight test of stable automated cruise flap for an adaptive wing aircraft. In *Journal of Aircraft,*, volume 47, pages 1178–1188, January 2009.

[21] D. Yeo, E. Atkins, L. Bernal, and W. Shyy. Aerodynamic sensing for a fixed wing uas operating at high angles of attack. In *Proc. AIAA Atmospheric Flight Mechanics Conference*, August 2012.

[22] N. Sydney, B. Smyth, and D. A. Paley. Dynamic control of autonomous quadrotor flight in an estimated wind field. In *Decision and Control (CDC), 2013 IEEE 52nd Annual Conference on*, pages 3609–3616, Dec 2013.

[23] K. Alexis, G. Nikolakopoulos, and A. Tzes. Experimental model predictive attitude tracking control of a quadrotor helicopter subject to wind-gusts. In *18th Mediterranean Conf. on Control Automation (MED), 2010*, pages 1461 –1466, June 2010.

[24] K. Alexis, G. Nikolakopoulos, and A. Tzes. Constrained-control of a quadrotor helicopter for trajectory tracking under wind-gust disturbances. In *MELECON 2010*, pages 1411 –1416, April 2010.

[25] C. Powers, D. Mellinger, A. Kushleyev, B. Kothmann, and V. Kumar. Influence of aerodynamics and proximity effects in quadrotor flight. In *Proc. of the Int. Symp. on Experimental Robotics*, June 2012.

[26] W. Khan and M. Nahon. Development and validation of a propeller slipstream model for small unmanned aerial vehicles. In *AIAA Journal of Aircraft*, April 2015.

[27] W. Khan and M. Nahon. Improvement and validation of a propeller slipstream model for small unmanned aerial vehicles. In *Proc. International Conference on Unmanned Aircraft Systems*, May 2014.

[28] F. White. *Viscous Fluid Flow*. McGraw-Hill Mechanical Engineering, 3 edition, January 2005.

[29] R. Jensen M. Albertson, Y. Dai and H. Rouse. Diffusion of submerged jets. In *Transactions* ,, volume 115, pages 639–697. American Society of Civil Engineers, 1950.

[30] D. Yeo. Performance and Slipstream Characteristics of Small-Scale Propellers at Low Reynolds Numbers. Master's thesis, Univ. of Illinois at UrbanaChampaign, Champaign, USA, 2014.

[31] D. Yeo, E. Shrestha, D. Paley, and E. Atkins. An empirical model of rotorcraft uav downwash for disturbance localization and avoidance. In *Proc. AIAA Atmospheric Flight Mechanics Conference*, January 2015.

[32] D. Yeo, N. Sydney, D. Paley, and D. Sofge. Onboard flow sensing for downwash detection and avoidance with a small quadrotor helicopter. In *Proc. AIAA Guidance Navigation and Control Conference*, January 2015.